Journal of Additive Manufacturing Technologies
DOI: 10.18416/JAMTECH.2111526

Infinite Science | Publishing

Effect of annealing conditions on microstructure and hardness of CoCrFeNiMn-0.18Ti high entropy alloy manufactured by electron beam melting

M. Cagirici[1,2], M.L.S. Nai[1], J. Wei[3], J. Ding[2] and P. Wang[1*]

[1] Singapore Institute of Manufacturing Technology, 73 Nanyang Drive, 637662, Singapore
[2] Department of Materials Science and Engineering, National University of Singapore, 117576, Singapore
[3] School of Materials Science and Engineering, Harbin Institute of Technology (Shenzhen), Shenzhen 518055, PR China
[*] Corresponding author, email: wangp@SIMTech.a-star.edu.sg

Abstract

The success of *in situ* alloying whilst developing high entropy alloys (HEAs) specific to the electron beam melting (EBM) process has been stated in the literature. Secondary phases forming on FCC matrix improved the mechanical properties of EBM-built; however, their random distribution limits the further improvement in mechanical performance. Herein, post-process heat treatments were designed to observe the effects on secondary phase morphology, distribution, and microhardness of EBM-built CoCrFeNiMn-0.18Ti HEA and establish the optimized heat treatments while reducing further cost. Systematic studies revealed that an increase in solutionizing time slightly enhanced the microhardness of the alloy despite the solutionizing temperature reversely affect the mechanical properties. On the one hand, reaching a solutionizing temperature of 1300°C would not be enough to dissolve all the secondary phases within a reasonable solutionizing time of two hours. Metastability of HEAs and the complex distribution of topologically formed secondary phases slowed down phase transformations through FCC matrix. On the other hand, the microhardness of samples was successfully reattributed at 600°C by annealing. Thirty minutes and fifteen hours of annealing improved the hardness of solutionized alloy by 58 and 150% while reaching 316 HV and 487 HV, respectively.

Keywords: Electron beam melting; High entropy alloys; Heat treatment; Thermal stability; Phase distribution

1. Introduction

High entropy alloys (HEAs) were firstly proposed by Cantor et al. and Yeh et al. in 2004 [1, 2]. HEAs have been intensively studied in recent years because of their inherent characteristics, such as exceptional solid solution forming capacity, outstanding mechanical performance, and excellent corrosion resistance [3-11]. The exceptional effects, having high entropy, severe lattice distortion, sluggish diffusion, and cocktail effect, attributed unique characteristics to HEAs [12]. HEAs mostly have a single-phase solid solution in the early studies due to the high configurational entropy of HEAs; however, the latter studies show that the mechanical or functional properties of HEAs could be modified by exploring promising alloys systems [13, 14]. The advances in manufacturing technologies also grasp the attention to tailor the properties of high entropy alloys [15-17].

Additive manufacturing (AM) technologies bring unbearable advantages such as short processing time, high geometrical accuracy, and near-net-shape processing [18, 19]. The most frequently used AM techniques for metal fabrication are selective laser melting (SLM) and electron beam melting (EBM), which utilized laser or electron beam as a power source while manufacturing parts layer by layer. Brif et al. and Fujieda et al. firstly fabricated CoCrFeNi and AlCoCrFeNi HEAs by SLM and EBM, respectively [20, 21]. The studies revealed that the mechanical properties of these HEAs fabricated by various additive manufacturing technologies yielded comparable or superior mechanical properties compared to the conventionally produced counterparts. Despite the fact that the firstly fabricated alloys contain single-phase solid solutions, the recently reported studies revealed that additively manufactured HEAs with outstanding properties were attributed by forming multi-phase structures including dual-phase and precipitation strengthened HEAs [3, 22-25]. On the other hand, the brittle precipitates weaken the mechanical properties of promising HEAs by decreasing their ductility. They also weaken the structural integrity by forming metallurgical defects. Therefore, post-processes are required to avoid the detrimental effects of precipitation.

Fujieda et al. stated that solution treatment improves the mechanical properties of SLMed $Co_{1.5}CrFeNi_{1.5}Ti_{0.5}Mo_{0.1}$ by dissolving brittle HCP precipitates [25]. On the other hand, forming and promoting nano precipitates in additively

manufactured HEAs contribute to exceptional mechanical performance without any deleterious effect [26]. Although constructive effects of post-processes have been reported in the literature, it was not explicitly studied employing recently developed AMed HEAs, having complex microstructural formations [3]. Therefore, we demonstrate the potential and advisable post-processes while investigating their effect on EBM-built CoCrFeNiMn-0.18Ti HEAs.

2. Material and methods

The designated amount of pure Ti powder (0.18 in molar ratio) was induced into pre-alloyed CoCrFeNiMn feedstock. *In situ* alloyed feedstock was used to manufacture the samples utilizing electron beam melting. Various sample geometries having dimensions of 15×15×10, 20×20×10, 10×90×10, and 15×90×10 mm^3 were successfully fabricated under a vacuum of 2×10^{-3} mbar. The process parameters of EBM were kept constant to avoid any irregular microstructural evolution rather than previous studies [3, 4]. Post-process heat treatments were designed to solutionize and anneal EBM-built CoCrFeNiMn-0.18Ti HEA. Carbolite tube furnace was utilized to follow designed heat treatment cycles, given in **Table 1**, under a protective atmosphere maintained by Argon gas. Solutionized and annealed samples were quenched into the water. The samples were prepared to have proper microstructural analysis and hardness tests. EBM-built and heat-treated samples were sectioned, prepared, and mirror-finished employing 1-3 µm diamond suspension followed by 0.05 µm colloidal silica. X-ray diffraction (XRD) analyses were conducted to investigate the phase constituents using Bruker AXS D8 Advance. Olympus MX51 optical microscope, energy-dispersive X-ray spectroscopy (EDS), and electron backscattered diffraction (EBSD) equipped Helios Nanolab 600 scanning electron microscope (SEM) were intensively used for microstructural characterization. Metallurgically prepared samples were also subjected to microhardness measurements at a load of 1000g with a dwell time of 15s employing Matsuzawa MMT-X3 Vickers hardness tester.

Table 1. Post-process heat treatment cycles for EBM-built CoCrFeNiMn-0.18Ti HEA.

Solutionizing		Annealing	
Temperature (°C)	**Time (mins)**	**Temperature (°C)**	**Time (mins)**
1100	120		
1200	120		
1300	120	600	10, 30, 90, 270, 900

3. Results and discussion

The microstructural and mechanical characterizations were conducted on the samples processed in three different solutionizing temperatures. It was revealed that the amount and distribution of secondary phases were changed according to the treatment conditions. Additionally, structural transformation and newly formed phases were detected by XRD (**Fig 1**). Sigma phase (CrFe) was dissolved entirely in all selected solutionizing conditions. On the other hand, Cr-rich laves phase could not be dissolved in the FCC matrix, although it structurally transformed from C14 to C15 structure. The solutionizing treatment activated the transformation of laves phase from hexagonal (C14) to cubic (C15) structure by inducing required activation energy [27, 28]. Moreover, an energetically favorable $NiTi_2$ phase was also observed solution treated and quenched samples. Dissolving HCP-structured Ni_3Ti phase observed in EBM-built CoCrFeNiMn-0.18Ti HEA caused the formation of FCC-structured $NiTi_2$ phase due to the instability of Ni_3Ti in the structure [29, 30].

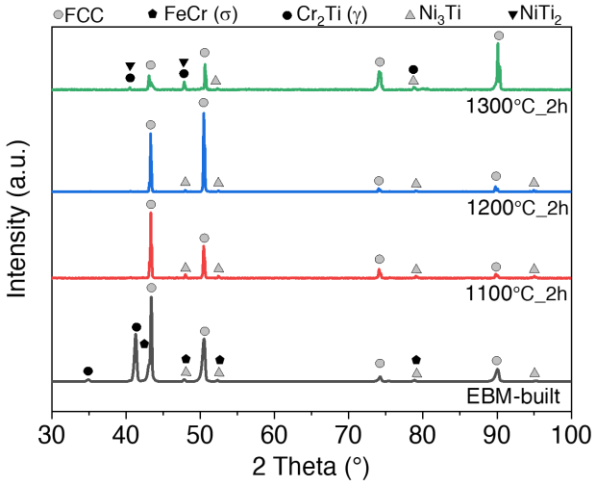

Fig 1. XRD patterns of EBM-built and solution treated CoCrFeNiMn-0.18Ti HEAs.

Optical microscopy images showed that the distribution and size of Cr_2Ti, Ni_3Ti, and $NiTi_2$ phases were changed with post-processing conditions. Despite the quantitative phase analysis were not conducted on each sample, differential interference contrast (DIC) imaging showed that existing secondary phases were randomly distributed in the structure (**Fig 2**). The amount of intermetallic precipitates decreased with increasing solutionizing temperature, as seen in **Fig 2**. Micron-sized precipitates were observed in the samples solutionized at 1100 and 1200°C for two hours. Further analysis based on observable grain boundaries revealed that the average size of precipitates was 3.79±1.78 µm in the sample subjected to solution treatment at 1200°C for 2h. Their existence was similar to topologically formed structures which were reported in the previous study [3]. Therefore, metallurgical defects were avoided in other samples subjected to solutionizing at high temperatures followed by annealing.

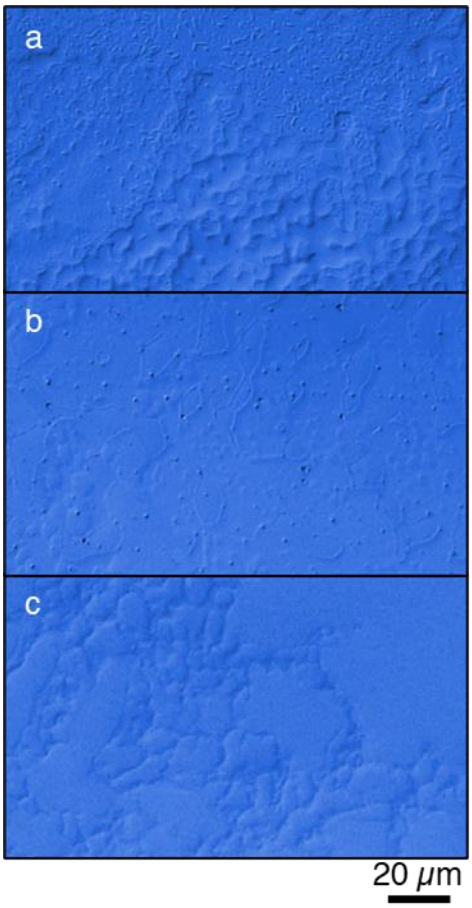

Fig 2. Optical microscopy images of solution-treated samples taken in DIC mode: a) 1100°C-2h, b) 1200°C-2h, and c) 1300°C-2h samples.

Furthermore, high-magnification microstructural characterization was conducted to reveal the compositional difference between matrix and precipitates as well as their distribution. **Fig 3** indicates that solutionizing heat treatment followed by quenching slowed down the growth of intermetallics while restricting their localization at the boundaries of FCC matrix. Despite DIC images (**Fig 2**) showed contrast difference between intermetallics and FCC matrix, EBSD analysis explicitly revealed their distribution by assigning the corresponding phases according to the particular crystal structure and Kikuchi pattern. Although Cr_2Ti and $NiTi_2$ phases were localized at FCC boundaries, EDS analysis showed that the topologically complex phases still exist in the sample (**Fig 3c**). Cr_2Ti intermetallics might be formed on top of previously dissolved σ-CrFe structures as the localization of Fe was also detected at the same region. Besides, the size of transformed Cr_2Ti precipitates, 1.46±0.62 μm, were slightly larger than the ones reported in C14 structure, 0.95±0.28 μm [3]. The solutionizing treatment, in fact, caused the growth of stable precipitates. Dissolving σ-CrFe and $D0_{24}$-Ni_3Ti also accelerated this growth by modifying the reaction kinetics. On the other hand, high entropy of CoCrFeNiMn-0.18Ti HEA promoted solid solution formation rather than promoting the nano-sized precipitate formation at the regions, including dissolved intermetallics. However, it should be noted that the resolution of EBSD analysis might not be able to observe any particles having a size below 150nm with current analysis settings.

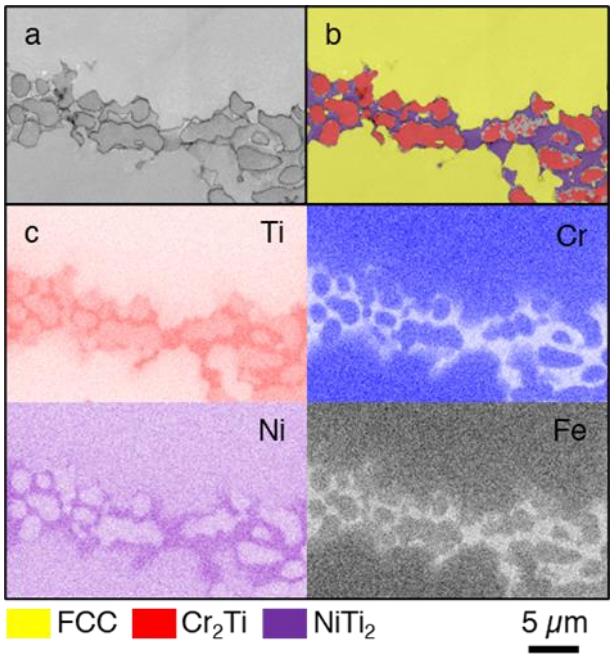

Fig 3. Microstructure of solution treated sample at 1300°C for two hours. a) Band contrast image, b) phase distribution maps, and c) EDS mappings showing the elemental distribution.

The mechanical properties of solutionized samples at different temperatures were investigated in terms of microhardness variation (**Fig 4**). Solution treatment at 1100°C only reduced the microhardness of EBM-built CoCrFeNiMn-0.18Ti HEA by ~20%. Increasing solutionizing temperature to 1200 and 1300°C caused a further decrease by 52 and 57%, respectively. Although XRD proved the existence of Cr_2Ti and $NiTi_2$ phases, they would not enhance the mechanical properties. On the contrary to EBM-built HEA, large size of these intermetallics solution treated samples could not contribute to the hardness of solution treated sample. Additionally, the decrease in intensity of XRD peaks belonging Cr_2Ti might also indicate that topologically complex structure partially dissolved. The growth of softer FCC matrix in solution treated sample decreased the resistance to deformation. It was seen that increase in annealing temperature at a constant time interval of 2 hours would not contribute to a further decrease in material hardness; however, it potentially contributes to the nucleation of nano precipitates once quenched. Thus, the solution-treated samples at 1300°C for 2h were annealed at 600°C to promote the growth of intermetallics/precipitates.

Moreover, the systematic works explored the effect of annealing time on microhardness. The hardness of solution-treated samples was improved by ~30 and 58% in a short time annealing of 10 and 30 mins, respectively. Although continuous increment in microhardness was expected, 90 and 270 mins

annealing only improved that by 8 and 24 HV1, respectively. Furthermore, the enhancement in microhardness was investigated by an extended annealing cycle of 15 hours. This treatment boosted the hardness value of solution-treated samples to 487±43 HV1.

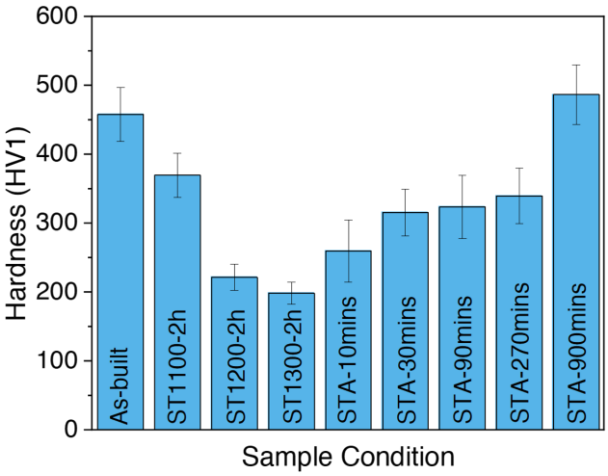

Fig 4. Microhardness of EBM-built and heat-treated samples. (ST: solution treated; STA: solution treated and annealed at 600°C)

4. Conclusions

In this study, we investigated the effects of post-process heat-treatments on microstructure and mechanical properties of EBM-built CoCrFeNiMn-0.18Ti HEAs. The following conclusions could be drawn by systematic study.

1. The topologically formed secondary phases in EBM-built alloy were partially dissolved in FCC matrix due to their stability at high temperatures.
2. Increasing solutionizing temperature (1300°C) further caused the change crystal structure of laves phase (C14→C15) and the formation of $NiTi_2$ intermetallics nearby the boundaries of FCC grains.
3. Annealing of solution-treated samples (ST1300-2h) at 600°C increased the hardness of CoCrNiFeMn-0.18Ti HEA. The significant enhancements, 50 and 100%, were achieved at ST1300-2h samples once they were annealed for 30 and 900mins, respectively.

This study formed a first guideline showing the effect of post-process conditions on in situ alloyed CoCrFeNiMn-0.18Ti HEA fabricated by EBM. The findings and methodology employed during this study might be used while tailoring the mechanical properties of multi-phase HEAs fabricated by EBM.

Acknowledgments

The work in the research was financially supported by the A*STAR Additive Manufacturing Centre (AMC) Initiative: Work Package 1 (High Temperature Materials Development for 3D Additive Manufacturing, Grant No. 1426800088).

Author's statement

Conflict of interest: Authors state no conflict of interest. Informed consent: Informed consent has been obtained from all individuals included in this study. Ethical approval: The research related to human use complies with all the relevant national regulations, institutional policies and was performed in accordance with the tenets of the Helsinki Declaration, and has been approved by the authors' institutional review board or equivalent committee.

References

1. Cantor, B., et al., *Microstructural development in equiatomic multicomponent alloys.* Matererials Science and Engineering A, 2004. **375-377**: p. 213-218.
2. Yeh, J.W., et al., *Nanostructured High-Entropy Alloys with Multiple Principal Elements: Novel Alloy Design Concepts and Outcomes.* Advanced Engineering Materials, 2004. **6**(5): p. 299-303.
3. Cagirici, M., et al., *Additive manufacturing of high-entropy alloys by thermophysical calculations and in situ alloying.* Journal of Materials Science & Technology, 2021. **94**: p. 53-66
4. Wang, P., et al., *Additively manufactured CoCrFeNiMn high-entropy alloy via pre-alloyed powder.* Materials & Design, 2019. **168**.
5. Cantor, B., *Multicomponent and High Entropy Alloys.* Entropy, 2014. **16**(9): p. 4749.
6. Yeh, J.W., *Recent progress in high entropy alloys.* Annales de Chimie Science des Matériaux, 2006. **31**(6): p. 633-648.
7. Liang, Y.-J., et al., *High-content ductile coherent nanoprecipitates achieve ultrastrong high-entropy alloys.* Nature Communications, 2018. **9**(1): p. 4063.
8. Lei, Z., et al., *Enhanced strength and ductility in a high-entropy alloy via ordered oxygen complexes.* Nature, 2018. **563**(7732): p. 546-550.
9. Shi, Y., B. Yang, and P.K. Liaw, *Corrosion-Resistant High-Entropy Alloys: A Review.* Metals, 2017. **7**(2): p. 43.
10. Miracle, D.B. and O.N. Senkov, *A critical review of high entropy alloys and related concepts.* Acta Materialia, 2017. **122**: p. 448-511.
11. Ye, Y.F., et al., *High-entropy alloy: challenges and prospects.* Materials Today, 2016. **19**(6): p. 349-362.
12. Tsai, K.Y., M.H. Tsai, and J.W. Yeh, *Sluggish diffusion in Co–Cr–Fe–Mn–Ni high-entropy alloys.* Acta Materialia, 2013. **61**(13): p. 4887-4897.
13. George, E.P., D. Raabe, and R.O. Ritchie, *High-entropy alloys.* Nat. Rev. Mater., 2019. **4**(8): p. 515-534.
14. Wang, X., W. Guo, and Y. Fu, *High-entropy alloys: emerging materials for advanced functional applications.* Journal of Materials Chemistry A, 2021. **9**(2): p. 663-701.
15. Ishimoto, T., et al., *Development of TiNbTaZrMo bio-high entropy alloy (BioHEA) super-solid solution by selective laser melting, and its improved mechanical property and biocompatibility.* Scripta Materialia, 2021. **194**.
16. Agrawal, P., et al., *Excellent strength-ductility synergy in metastable high entropy alloy by laser powder bed additive manufacturing.* Additive Manufacturing, 2020. **32**: p. 101098.
17. Chen, S., Y. Tong, and P. Liaw, *Additive Manufacturing of High-Entropy Alloys: A Review.* Entropy, 2018. **20**(12): p. 937.
18. Wang, P., et al., *Additively manufactured heterogeneously porous metallic bone with biostructural functions and bone-like mechanical properties.* Journal of Materials Science & Technology, 2021. **62**: p. 173-179.
19. Wang, P., et al., *Experimental analysis of additively manufactured component and design guidelines for*

lightweight structures: A case study using electron beam melting. Additive Manufacturing, 2020. **33**: p. 101088.
20. Brif, Y., M. Thomas, and I. Todd, *The use of high-entropy alloys in additive manufacturing.* Scripta Materialia, 2015. **99**: p. 93-96.
21. Fujieda, T., et al., *First demonstration of promising selective electron beam melting method for utilizing high-entropy alloys as engineering materials.* Mater. Lett., 2015. **159**: p. 12-15.
22. Wang, Y., et al., *Microstructures and properties of equimolar AlCoCrCuFeNi high-entropy alloy additively manufactured by selective laser melting.* Intermetallics, 2020. **120**: p. 106746.
23. Malatji, N., et al., *Tribological and corrosion properties of laser additive manufactured AlCrFeNiCu high entropy alloy.* Materials Today: Proceedings, 2020.
24. Guan, S., et al., *Additively manufactured CrMnFeCoNi/AlCoCrFeNiTi0.5 laminated high-entropy alloy with enhanced strength-plasticity synergy.* Scripta Materialia, 2020. **183**: p. 133-138.
25. Fujieda, T., et al., *Mechanical and corrosion properties of CoCrFeNiTi-based high-entropy alloy additive manufactured using selective laser melting.* Additive Manufacturing, 2019. **25**: p. 412-420.
26. Wu, W., et al., *Nano-sized precipitates and dislocation networks reinforced C-containing CoCrFeNi high-entropy alloy fabricated by selective laser melting.* Materials Characterization, 2018. **144**: p. 605-610.
27. Tsai, M.-H., et al., *Intermetallic Phases in High-Entropy Alloys: Statistical Analysis of their Prevalence and Structural Inheritance.* Metals, 2019. **9**(2): p. 247.
28. Aufrecht, J., A. Leineweber, and E.J. Mittemeijer, *Polytypic transformations of the $HfCr_2$ Laves phase – Part II: Kinetics of the polymorphic C14 → C15 transformation*. Intermetallics, 2011. **19**(10): p. 1442-1447.
29. Yeh, A.-C., et al., *On the Solidification and Phase Stability of a Co-Cr-Fe-Ni-Ti High-Entropy Alloy*. Metallurgical and Materials Transactions A, 2014. 45(1): p. 184-190.
30. Pasturel, A., et al., *Electronic structure and phase stability study in the Ni-Ti system.* Physical Review B, 1995. **52**(21): p. 15176-15190.